



HAL
open science

On the Influence of the Protonation States of Active Site Residues on AChE Reactivation: A QM/MM Approach

Thomas Driant, Florian Nachon, Cyril Ollivier, Pierre-Yves Renard, Etienne Derat

► To cite this version:

Thomas Driant, Florian Nachon, Cyril Ollivier, Pierre-Yves Renard, Etienne Derat. On the Influence of the Protonation States of Active Site Residues on AChE Reactivation: A QM/MM Approach. *ChemBioChem*, 2017, 18 (7), pp.666-675. 10.1002/cbic.201600646 . hal-01644385

HAL Id: hal-01644385

<https://hal.science/hal-01644385v1>

Submitted on 8 Jan 2018

HAL is a multi-disciplinary open access archive for the deposit and dissemination of scientific research documents, whether they are published or not. The documents may come from teaching and research institutions in France or abroad, or from public or private research centers.

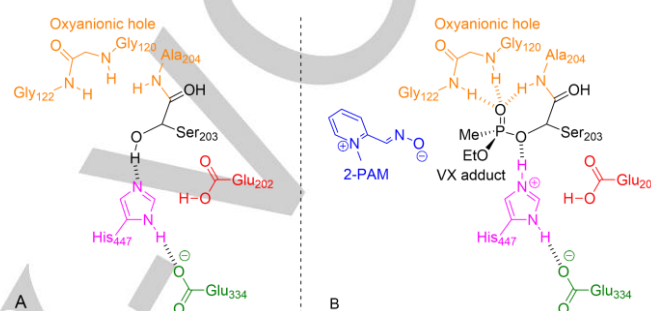
L'archive ouverte pluridisciplinaire **HAL**, est destinée au dépôt et à la diffusion de documents scientifiques de niveau recherche, publiés ou non, émanant des établissements d'enseignement et de recherche français ou étrangers, des laboratoires publics ou privés.

On the influence of the protonation states of active site residues on AChE reactivation: a QM/MM approach

Thomas Driant^[a], Florian Nachon^[b], Cyril Ollivier^[a], Pierre-Yves Renard^[c], Etienne Derat^{*[a]}

Abstract: Acetylcholinesterase (AChE) is an enzyme of the serine hydrolase superfamily and a mediator of the signal transmission at cholinergic synapses catalysing acetylcholine cleavage into an acetate and a choline. This enzyme is vulnerable to covalent inhibition by organophosphate compounds. The covalent inhibition of AChE does not revert spontaneously and in order to restore catalytic activity known reactivator compounds have limited action. Simulations of VX-inhibited AChE reactivation by pralidoxime, a classical reactivator, were performed by QM/MM. These simulations allowed for a broader view of the effect of protonation states of active site residues. These calculations provide evidence for the role of Glu202, which needs to be protonated for reactivation to occur. In situ deprotonation of 2-PAM was also explored in both protonation states of Glu202, showing that His447 is able to deprotonate 2-PAM with the assistance of Glu202. Since the active site of serine hydrolases is highly conserved, this work shades new insights on the interplay between the triad residues of the catalytic center and this glutamate newly identified as protonatable.

as well as many aromatic or positively charged inhibitors.^[4–6] Next to the catalytic serine, an oxyanion formed by the main chain nitrogens of Gly121/Gly122/Ala204 (see Scheme 1) stabilizes transition states during catalysis.^[7]

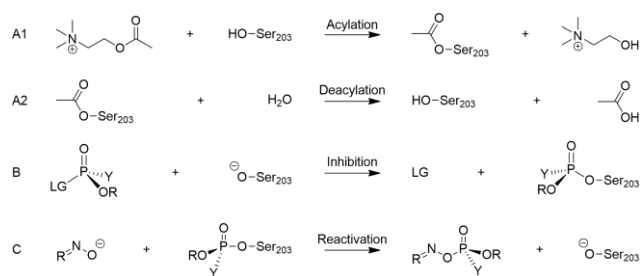


Scheme 1. Main active site residues of inhibited AChE coloured in the colouring scheme used throughout the article. Note that in this scheme the catalytic serine is inhibited by VX.

Introduction

The main role of acetylcholinesterase (AChE, EC 3.1.1.7) is the termination of nerve signal transmission at cholinergic synapses by catalysis of the hydrolysis of the neurotransmitter acetylcholine (ACh). The crystal structure of human AChE revealed that the catalytic triad Ser203/His447/Glu334 (see Scheme 1A) is located at the bottom of a 20-Å deep narrow gorge lined by aromatic residues.^[1–3] These aromatic residues control the access to the gorge, the binding specificity and orientation of substrates and inhibitors. For example, Trp286, Tyr124 and Tyr72 located at the gorge entrance form an aromatic cluster called the peripheral site, which binds ACh transiently on its way down to the gorge,

Noteworthy, an extensive hydrogen bond network interconnects structural water molecules and residues in the gorge to the catalytic triad.^[8] The regular catalytic cycle of AChE (hydrolysis of ACh) involves two steps (Scheme 2, A1 & A2). During the acylation step, the nucleophilic Ser203 attacks the ester group of ACh, yielding the acetylated serine and elimination of choline. During the deacylation step, a water molecule regenerates Ser203 and liberates acetic acid.



Scheme 2. Chemical equations of main processes of AChE. A1 and A2 are the acylation and deacylation steps or the normal catalytic activity of AChE. B is the inhibition by organophosphate compound. C is the reactivation of inhibited AChE.

The acute toxicity of organophosphorus nerve agents results from the irreversible inhibition of AChE through phosphorylation of its catalytic serine (Scheme 2B).^[9] Water induced dephosphorylation of this serine residue is by far slower than

[a] T. Driant, C. Ollivier, E. Derat
Sorbonne Universités, UPMC UNIV Paris 06, Institut Parisien de Chimie Moléculaire, UMR CNRS 8232, Case 229, 4 Place Jussieu, 75252 Paris Cedex 05, France

[b] F. Nachon
Département de Toxicologie et Risques Chimiques, Institut de Recherche Biomédicale des Armées, 1 Place Général Valérie André, 91223 Brétigny-sur-Orge Cédex, France

[c] P.-Y. Renard
Normandie Univ, COBRA, UMR 6014 & FR 3038; Univ Rouen - Normandie; INSA Rouen; CNRS, 1 rue Tesnière 76821 Mont-Saint-Aignan, Cedex (France)

Additional tables and Figures mentioned in the main text, list of atoms in the QM and MM zones, energy of all mentioned structures and xyz coordinates for the QM zone of all mentioned structures. (PDF)

deacylation.^[3,10] Subsequent accumulation of ACh at neuronal synapses and neuromuscular junctions, results in paralysis, seizures and other symptoms of cholinergic syndrome, and lead to death by respiratory arrest. Phosphorylated AChE can be reactivated by nucleophilic agents such as oximes (Scheme 2C).^[11] Reactivation restores the catalytic activity. The current molecules used for emergency treatment of nerve agent poisoning are pyridinium aldoximes, 2-PAM (pralidoxime; 2-[(hydroxyimino)methyl]-1-methylpyridin-1-ium), HI-6 (4-carbamoyl-1-[(2-[(*E*)-(hydroxyimino)methyl]pyridinium-1-yl)methoxy)methyl]pyridinium) and obidoxime (1,1'-[oxybis(methylene)]bis[4-[(*E*)-(hydroxyimino)methyl]pyridinium]). Unfortunately, they are not efficient against all known nerve agents and poorly cross the blood brain barrier to reactivate AChE in the central nervous system. As a universal antidote is still lacking, new efforts have been made in the recent years to design more efficient reactivators.^[11]

Efficient molecular design of better reactivators requires a good knowledge of both AChE structure and reactivation mechanism. Yet important factors, e.g. the geometry of the nucleophilic attack or simply the protonation state of catalytic residues and the reactivator during the reaction, remain largely unknown.^[12] Crystallographic data have failed to provide a clear answer to these questions so far, so that theoretical calculations become a method of choice. For that matter, AChE has already been the subject of multiple computational studies.

The catalytic cycle of AChE leading to the splitting of acetylcholine has been investigated computationally by various groups. McCammon has in particular demonstrated the importance of the oxyanion hole for stabilizing the key transition state and tetravalent intermediate.^[13] This mechanism was later supported by Born-Oppenheimer molecular dynamics within a QM/MM framework, emphasizing the role of proton transfer between the partners of the catalytic triad.^[14] The role of Glu202 for the orientation of the nucleophilic water molecule during the second stage of the catalytic cycle was highlighted in a QM/MM study from the Nemukhin group.^[15] Recently, Fattbert et al. performed a QM molecular dynamics study with a large QM region: they found that the second step of the acylation is the rate-determining step.^[16]

The specific problem of AChE phosphorylation by nerve agents was also investigated by means of theoretical methods. In 2008, a model QM study substantiated the hypothesis that inhibition occurs via an addition-elimination process.^[17] Our group demonstrated through QM/MM calculations that the leaving group of the covalent inhibitor (namely the cyano moiety of organophosphate inhibitor known as tabun) can be expelled more easily when situated in *syn* position of the catalytic serine residue.^[18] This last result shows that textbooks' mechanism can be reevaluated by QM/MM calculations. The investigative power of static QM/MM methodology has yielded stimulating results on a large array of enzymatic reactions.^[19,20]

Several groups have also investigated catalytic profiles of AChE reactivation by oximes. Through QM/MM calculations, it was shown that Glu334 stabilizes the pentavalent intermediate during the reactivation.^[21] The group of Ganguly evaluated through QM only calculations various reactivators and showed

that neutral ones are kinetically more efficient.^[22] Later, they demonstrate that the rate-limiting step is different for charged pyridinium oximes and non-charged pyridine oximes: both species process through an addition-elimination mechanism. For charged species, the rate-determining step is the elimination while it is the addition for non-charged.^[23] It was also demonstrated by semi-empirical QM/MM calculations that the peripheral site moiety of the active site is helpful to bind the reactivator and to stabilize the key transition state.^[24] Recent QM/MM calculations have concluded to the possibility of deprotonating an oxime by His447, previous to the standard addition-elimination mechanism.^[25] But they did not investigate all the protonation states of the various acidic residues. With unprotonated Glu202, it was shown by QM/MM FEP (Free Energy Perturbation) that reactivation by a water molecule coming from the gorge is a worthwhile hypothesis.^[26]

The importance of Glu202 to the reactivation process was uncovered in a paper by Quinn and coworkers.^[27] A Glu202Gln mutation was performed that severely decreased the binding and reactivation activity of 2-PAM. This mutation was shown to have no effect on the geometry of the active site. The reason for the change in reactivity was not investigated at that time.

To summarize the current achievements, proton transfers are clearly key features to understand the reactivation process: all the residues surrounding the phosphorus center can be either protonated or unprotonated (His447, Glu334, Glu202). Similarly, the strong α -nucleophiles (i.e oximes) used to reactivate can enter the active site under either protonated state, depending of the local pH and the pKa of the considered oxime. But a unified approach combining reactivation/protonation states based on QM/MM simulations is still lacking. Our first question is thus the following: how does the protonation state of Glu202 influence the reactivation of VX-inhibited AChE by unprotonated pralidoxime? In a second step, and based on the results obtained by answering our first question, examination of pralidoxime deprotonation will be completed. The protonation states effect on the reactivation will then be unified in a single scheme.

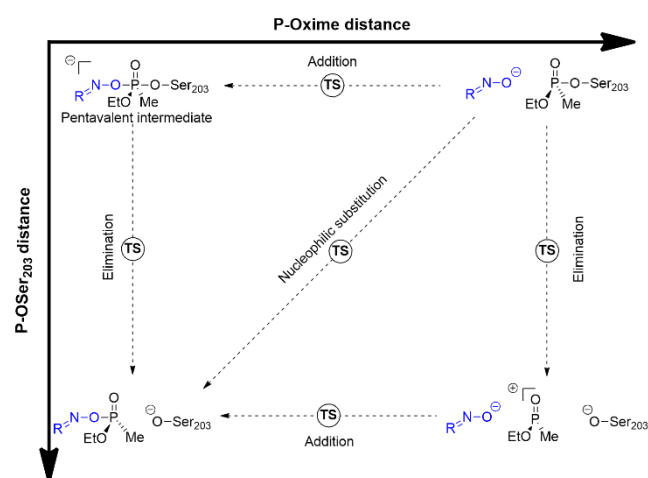


Figure 1. Envisaged mechanisms for reactivation depending on phosphorus-oxime distance and phosphorus-Ser203 distance. Since phosphorus can accommodate various geometrical patterns (ranging from 3 to 6 substituents), one can imagine different mechanisms for this reaction. Figure 1 presents plausible mechanisms for the reactivation of VX inhibited AChE by pralidoxime.

The most obvious mechanism for the reactivation is a nucleophilic substitution of the second order. This mechanism is obviously single step with no reaction intermediate. There is a single transition state in which the phosphorus-oxime and phosphorus-Ser203 bond distance are expected to be roughly equivalent due to both being single P-O bonds. Since phosphorus can be hypervalent a two-step addition elimination mechanism with a hypervalent intermediate is also plausible. The first step is an addition, namely the nucleophilic attack of the oxime on the phosphorus. During this step the phosphorus-oxime distance is shortened to the length of a P-O covalent bond. The length of the phosphorus-Ser203 bond remains roughly the same. This addition leads to the formation of a pentavalent intermediate with short phosphorus-oxime and phosphorus-Ser203 distances. This intermediate is negatively charged and thus can be stabilized by the oxyanion hole. Then the elimination step takes place in which the leaving group (Ser203) departs. The phosphorus-Ser203 distance is elongated and the phosphorus-Ser203 covalent bond broken while the phosphorus-oxime distance remains constant.

The third possible mechanism is the elimination-addition two-step mechanism. First there is the elongation of the phosphorus-Ser203 bond but at the same time the phosphorus-oxime bond is not formed, it is the elimination step. The phosphorus-oxime distance does not change during this step. At the end of this step an intermediate is obtained. This intermediate is the resulting cation after the abstraction of an alkoxy group from an organophosphate. In this intermediate one can consider that the phosphorus moiety is positively charged while surrounded by two negatively charged oxygens (oximate and serine alcoholate). The second step is the addition step with the nucleophilic attack of the oximate on the phosphorus. During this step the phosphorus-oxime distance is shortened to that of a covalent bond. We found absolutely no evidence to support this mechanism and discarded it in the following discussion.

Computational Details

The 3DL7^[28] PDB structure of the tabun-phosphorylated enzyme with bound 2-PAM is the starting point of this work. Of the two monomers present in the original PDB only one is kept with all water molecules in proximity. The ligands and a chloride ion, necessary to the crystallization, are deleted. Tabun was replaced by VX. A list of the decisions made on residues where crystallographic data were inconclusive can be found in the supporting information file.

The CHARMM22^[29,30] parameters are used with the CHARMM^[31] software to add hydrogens to the crystallographic structure and optimize their position. A 8 Å thick layer of water molecules is added around AChE with Chimera 1.10.1.^[32] The

entire enzyme, minus the catalytic triad kept frozen, is then entirely relaxed by molecular mechanics using CHARMM with CHARMM22 parameters. The PROPKA^[33] software is used to calculate theoretical pKas for residues with an acidic or basic side chain, and then to attribute protonation states for relevant residues, especially all the histidines (See Supplemental Table 1). Nevertheless for key reactive residues in the active site, protonation will be discussed later on the basis of QM/MM calculations. The enzyme has an overall charge of -8. Thus, 8 water molecules are replaced by 8 sodium ions near negatively charged residues on the enzyme's surface. Finally, a short (5ns) molecular dynamic is performed in order to relax the system and verify its stability.

QM/MM is used in order to study the reactivity in AChE's active site while taking the apoenzyme into account. The QM zone (see Figure 2) includes the inhibited catalytic triad, comprised of the Ser203-VX adduct (except the nitrogen of the peptide chain), the imidazole cycle of His447 and the acetate of Glu334. The role of these last two residues is heavily documented in the literature and our QM setup follows the admitted protonation state.^[14] Moreover, QM/MM allows this proton to freely transfer between Glu334 and His447. The oxyanionic hole is also present in the QM zone. It includes Gly121, the carbonyl of Gly120, the amine and alpha carbon of Gly122, Ala204 and the amine and alpha carbon of Gly205. Are also included 2-PAM, the reactivator, and in some calculations, the acetate of Glu202. There are in total ninety atoms in the QM zone when Glu202 is included, 84 when it is not. The optimized MM zone contains all the atoms of the QM area. It also contains nineteen water molecules and aromatic residues of the enzyme gorge. Also present in the MM zone are residues and two water molecules forming a network of hydrogen bonds with Glu334 (Glu202, Glu450, Ser229 and Tyr428). The exhaustive list of atoms included in the MM zone can be found in the supporting information file (353 atoms in total). The rest of the enzyme and the water molecules surrounding it are treated in MM but not optimized. Of course, the whole MM part is polarizing the QM area via an electrostatic embedding scheme including the charge shift correction^[34].

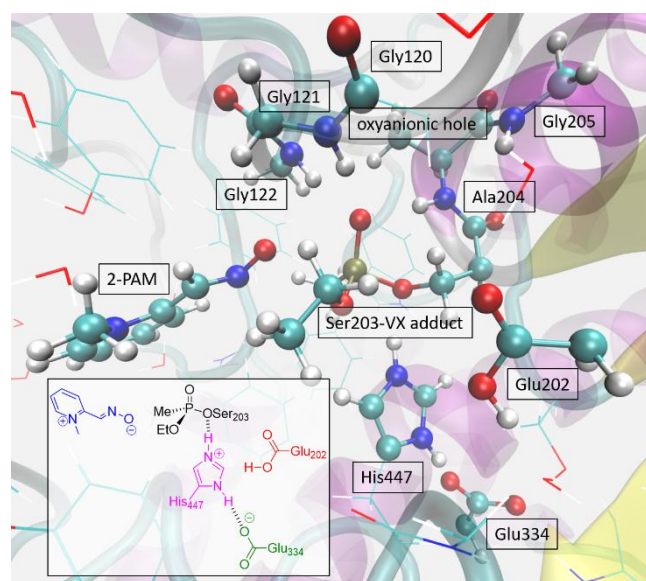


Figure 2. Optimised structure of the reactant for the reactivation of VX inhibited AChE by 2-PAM. The residues of the QM zone are in Ball&Stick representation. The optimized MM zone is in line representation. The rest of the enzyme, treated by MM but not optimized, is represented by ribbons coloured by secondary structure. For sake of simplicity, a 2D drawing is added with a residue coloring scheme that will be used throughout the article.

The geometries are optimized with the HDLCOpt module included in Chemshell 3.1b1.^[34] The QM energetical data is provided by Turbomole V6.4^[35,36] with the DFT functional B3LYP^[37,38] and the dispersion correction D3^[39]. The def2-SV(P)^[40] basis set is used except for phosphorus, the oximate function of 2-PAM and the three oxygens bound to phosphorus in the Ser203-VX adduct. For those atoms, the def2-SVPD basis set is used. The MM data is provided by the DL_POLY_3 interface present in Chemshell based on the CHARM22 parameters. The scans are performed with the scripting tools available in Chemshell. All stationary points and transition states are localized by full geometry optimizations. Then, two series of single points (SP) are performed: one with Turbomole at B3LYP-D3 level with the def2-TZVP basis set and the second with ORCA^[41] at DLPNO-CCSD(T)^[42,43] level with the def2-TZVPP basis set in order to verify the accuracy of the DFT calculations. The energy is then added to the MM energy provided by Chemshell to obtain a QM/MM energy for comparison purposes. With the two sets of B3LYP-D3 calculations, basis set convergence can be esteemed. The DLPNO-CCSD(T) methodology has been shown to have an accuracy of 1 kcal/mol (on the FH and S66 test sets) with the NormalPNO setting that was used in our work.^[44]

Results and Discussion

In the literature, the reactivation of AChE is generally modeled with an unprotonated Glu202. Another issue is the approach of 2-PAM towards the phosphorus center. Two

possibilities can be envisaged: the oxime being in trans configuration relative to Ser203 or the oxime being in trans configuration to the phosphoryl bond (see SI). QM/MM calculations on both approaches reveal that the second one is unfavorable (Supplemental Figure 3) due to steric interactions between 2-PAM and Tyr337/Phe338. Moreover, the oxyanionic hydrogen bond network is not well suited to accommodate this attack. Thus, we will disregard in the following this second approach to focus on the first one.

To localize the approximate transition state of this reaction a monodimensional energy scan with a fixed phosphorus-oxime distance and a relaxed phosphorus-Ser203 distance was performed. The results of the monodimensional scan did not allow us to obtain reliable energy barriers. Thus, a bidimensional scan was performed with both phosphorus-oxime and phosphorus-Ser203 distances controlled and scanned by 0.05 Å steps (Figure 3). A total of 251 points were gathered, all optimized in B3LYP-D3 with the def2-SV(P) basis set. A three-dimensional potential energy surface was obtained, the first two dimensions being reaction coordinates (phosphorus-oxime distance and phosphorus-Ser203 distance) and the third being the energy (Figure 3a). The start of the reaction, the reactant, is called structure **1** (Figure 3b) in the top right corner of the potential energy surface (Figure 3a). In this structure we have a covalent bond between the phosphorus and Ser203 while the oxime is 2.904 Å from the phosphorus (Figure 3b). The bidimensional scan was not performed up to a phosphorus-oxime distance of 2.904 Å but only up to a phosphorus-oxime distance of 2.561 Å. A monodimensional scan was performed between the reactant and the start of the bidimensional scan which indicated only very little energy variation in that section. Where the scan starts (green area in the top right) the energy is between 2.00 and 4.00 kcal.mol⁻¹ higher than the reactant's energy. This energy increases linearly when the phosphorus-oxime distance is shortened and the phosphorus-Ser203 distance is fixed. In that first section if the phosphorus-Ser203 is increased the energy rises very quickly. When the phosphorus-oxime distance is 1.85 Å shortening that distance results in a sudden rise of the energy. When this distance does not vary and the phosphorus-Ser203 distance is lengthened, the energy increases as well but much slower until structure **TS1-2** (phosphorus-oxime distance of 1.821 Å and phosphorus-Ser203 distance of 2.171 Å see Figure 3b) is reached. When the phosphorus-Ser203 distance is increased after **TS1-2** the energy decreases slightly until structure **2**, the reaction product, is reached.

This potential energy surface with a single step reaction and a single transition state indicates a S_N2 mechanism. But as was explained in the introduction, the transition state of an S_N2 is characterized by roughly equal distances between leaving group and central atom and nucleophile and central atom. In the **TS1-2** structure (Figure 3b) the oxime-phosphorus distance is short, 1.821 Å, very similar to the distance found in covalent bond of the product (**2**) (1.753 Å). The phosphorus-Ser203 distance is 2.171 Å, much longer than the distance found in covalent bond found in the reactant (**1**) (1.648 Å). The transition state geometry is thus very distinct from the near symmetrical shape expected

in a transition state of an S_N2 . It is much closer to the expected geometry for the transition state of the elimination step of an addition-elimination mechanism. The evolution of both bond lengths does not reflect the simultaneity of bond breaking and formation expected in a S_N2 reaction. Only one reaction distance varies at a time; first the phosphorus-oxime (nucleophile) for the addition step then the phosphorus-Ser203 (leaving group) for the elimination step. This is characteristic of an addition-elimination reaction. **TS1-2** is the transition state for the elimination step. We were unable to find neither the stable intermediate of the addition-elimination nor the transition state of the addition step. This can be explained by a very small energy barrier for this particular addition step. The reactivation of AChE by 2-PAM when Glu202 is unprotonated thus seems to go through addition-elimination mechanism.

Due to the well-documented underestimation of the activation barrier for S_N2 by B3LYP,^[45] an ab-initio DLPNO-CCSD(T) single point was performed in order to ascertain the quality of the B3LYP data. But first, B3LYP-D3 single point energetics with a bigger basis set were conducted. At the B3LYP-D3/def2-TZVP//CHARMM level the reaction is endothermic with the product's (**2**) energy higher than that of the reactant (**1**) by 17.00 kcal.mol⁻¹. At the same level, the energy barrier is 18.90 kcal.mol⁻¹. Finally, the DLPNO-CCSD(T)/def2-TZVPP single points show an endothermic reaction (by 9.55 kcal.mol⁻¹) with a 17.49 kcal.mol⁻¹ barrier. They reproduce the trend of DFT calculations and therefore corroborate their reliability. This energy barrier is not too high for AChE to overcome, but the endothermicity prevents reactivation in this protonation state situation by microreversibility.

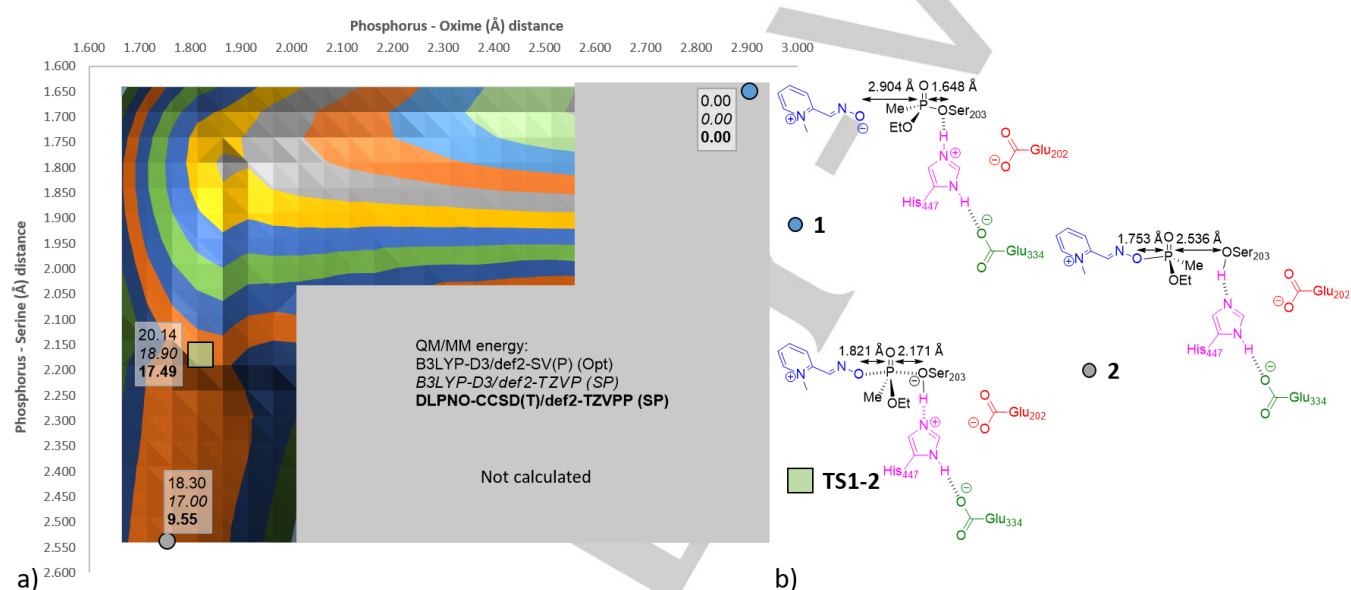


Figure 3. Reactivation of AChE with unprotonated Glu202 a) Potential energy surface as a function of the distance between the phosphorus and Ser203 and the distance between the phosphorus and 2-PAM. The position of the key geometries is highlighted with the energy in kcal.mol⁻¹ b) Key geometries. Distances in Angström.

Both The high endothermicity and the high-energy barriers indicate that reactivation is not possible in the case of unprotonated Glu202. Thus a new protonation state should be envisaged for this residue. This time Glu202 is protonated. Since a bidimensional scan had to be resorted to for the unprotonated Glu202 case a bidimensional scan was also used for protonated Glu202. Again both phosphorus-oxime and phosphorus-Ser203 distances are controlled and scanned by 0.05 Å steps (Figure 4). This time 282 points were gathered, all optimized in B3LYP-D3 with def2-SV(P). The potential energy surface that was obtained is three dimensional, two dimensions being reaction coordinates (phosphorus-oxime distance and phosphorus-Ser203 distance) and the third being the energy (Figure 4a). The reactivation starts at the top right corner of the potential energy surface with structure **1P**. The scan only starts at a phosphorus-oxime

distance of 2.571 Å. This distance is 2.752 Å in the reactant **1P**. A monodimensional scan was performed between the reactant and the start of the bidimensional scan which indicated that there is almost no energy variation in that section. The scan starts with a large gray area, which indicates an energy that is between 0.00 and 2.00 kcal.mol⁻¹ higher than the reactant's energy. When the phosphorus-Ser203 distance is lengthened from the start of the reaction, the energy increases rapidly. When this distance is kept fixed and the phosphorus-oxime distance is shortened, the energy remains in the flat green section of the potential energy surface. When the phosphorus-oxime distance is lengthened from 2.571 Å to 2.069 Å a stable reaction intermediate (**1P**) is found (Figure 4b). This reaction intermediate has an energy of 1.35 kcal.mol⁻¹ in def2-SV(P). From this intermediate if the phosphorus-Ser203 is lengthened

the energy also increases, albeit slowly. When the phosphorus-oxime distance is shortened the energy remains in the 0.00-2.00 area. After the phosphorus-oxime distance reaches 1.85 Å the energy starts to increase as the distance is pushed shorter. If the phosphorus-Ser203 distance is the one being lengthened, the energy also does increase but much slower. The increase in phosphorus-Ser203 distance brings us to a saddle point (**TS1P-2P**). After this saddle point if the phosphorus-Ser203 distance is lengthened further the energy decreases until it reaches structure **2P**, the product.

The potential energy surface is reminiscent of a two-step mechanism with a stable intermediate in between. We were unable to find the energy barrier for the first step between the reactant (**1P**) and the stable intermediate (**1*P**) due to the flatness of the surface. The stable intermediate is the

pentavalent structure expected for an addition-elimination mechanism on a phosphorus center. It is distorted with a much longer phosphorus-oxime distance (2.069 Å) than the phosphorus-Ser203 distance (1.760 Å) (Figure 4b) where a more symmetrical intermediate could be expected. The **TS1P-2P** structure with its long phosphorus-Ser203 distance (2.111 Å) and the much shorter phosphorus-oxime distance (1.791 Å) is the transition state of the elimination step. In that case again the evolution of both bond length is not simultaneous but happens in sequence. The mechanism of the reactivation of AChE with 2-PAM and protonated Glu202 seems to be an addition-elimination mechanism. We were unable to identify the energy barrier for the addition step and we thus hypothesize that this first step is nearly barrierless.

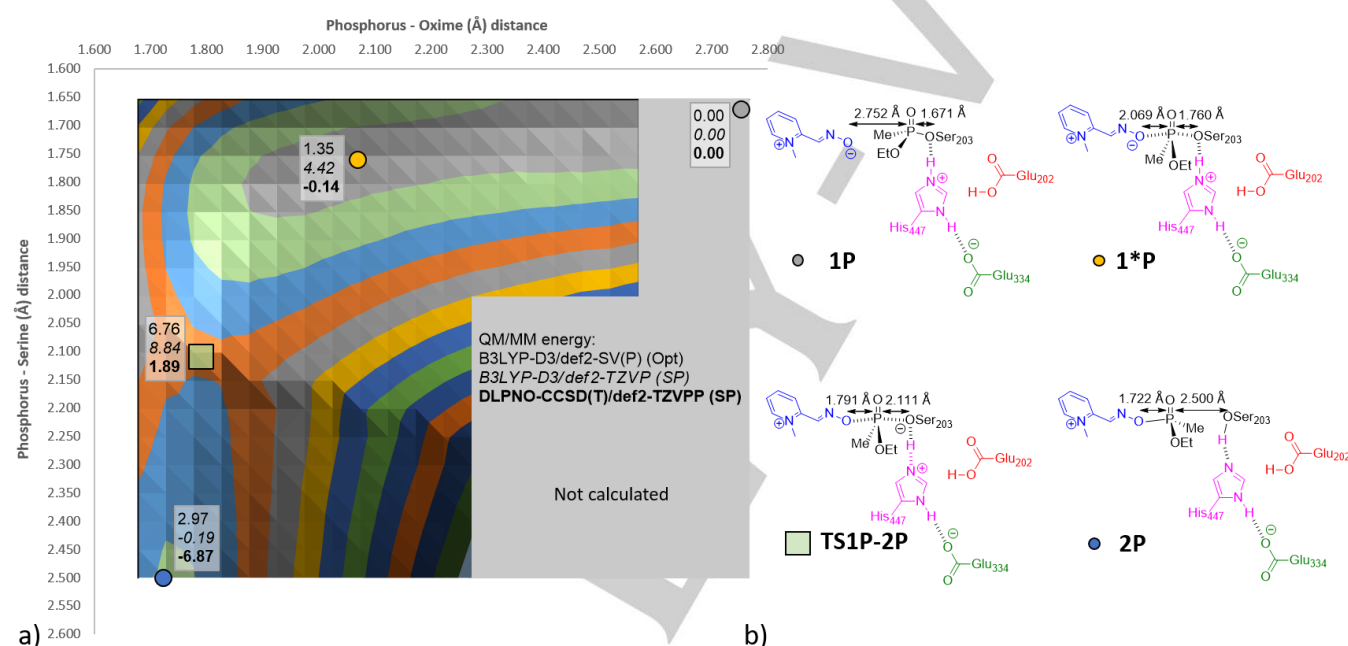


Figure 4. Reactivation of AChE with protonated Glu202 a) Potential energy surface as a function of the distance between the phosphorus and Ser203 and the distance between the phosphorus and 2-PAM. The position of key geometries is pointed with the energies in kcal.mol⁻¹. b) Key geometries, Distances in Angström.

At the B3LYP-D3/def2-TZVP//CHARMM level the reactivation of AChE by 2-PAM is isoenergetic with a very small energy gain of 0.19 kcal.mol⁻¹ (Figure 4a). The energy barrier of reactivation is 8.84 kcal.mol⁻¹. The DLPNO-CCSD(T) single points show the same trend with an energy gain of -6.87 kcal.mol⁻¹ and a small reaction barrier of 1.89 kcal.mol⁻¹. The reliability of the DFT calculations is once again confirmed. This case, contrary to the unprotonated Glu202 case, thus leads to reactivation. The energy barrier is small enough and the enthalpy is close to zero.

Those results and the effect of the protonation state of Glu202 on the reactivation has been evaluated by a cluster QM methodology. We hypothesize that an unprotonated Glu202 inhibits the reactivation by a negatively charged species arriving in the vicinity from the opposite direction, because it creates a

strong electrostatic repulsion. By removing all other interactions coming from the MM area in a cluster approach, it is expected to recover Glu202's effects. This approach is described in greater details in the supplementary material (SI Figure S6, S7, S8 and following paragraphs). This cluster QM method shows that with a protonated Glu202, the reactivation has an endothermicity of 4.11 kcal.mol⁻¹ and a barrier of 6.96 kcal.mol⁻¹. On the other hand, when Glu202 is unprotonated, the endothermicity is much higher at 23.92 kcal.mol⁻¹ and so is the reaction barrier at 24.01 kcal.mol⁻¹. It confirms that the trends observed in QM both in terms of the reaction barrier and the energy difference between reactant and product are due to the protonation state of Glu202. These two sets of calculations (QM and QM/MM) demonstrate that the presence of a negative charge in close proximity with

the Ser203-VX adduct repels the approach of a negatively charged oxime, thus preventing reactivation.

Since Glu202 needs to be protonated for reactivation to occur, from where is the proton coming? 2-PAM could act as a proton donor in the active site. Indeed, the oxime can only reactivate AChE in its oximate form and thus needs to lose a proton. With an experimental pKa of 7.68 in physiological conditions, 2-PAM can be deprotonated either before entering the active site of AChE, or in the active site. It was thus decided to study how 2-PAM could be deprotonated in the active site by His447 when Glu202 is protonated and when it is unprotonated.

The deprotonation of 2-PAM by His447 when Glu202 is unprotonated is presented in Figure 5a. This deprotonation is a one-step exothermic reaction with a gain of 3.22 kcal.mol⁻¹. The

energy barrier is 11.46 kcal.mol⁻¹. A stable intermediate (4*) was optimized between the reactant (4) and the transition state (TS4-1). It has an energy of 7.30 kcal.mol⁻¹, higher than the reactant. No energy barrier could be found between the reactant and this intermediate. When 2-PAM approaches His447 it forms a hydrogen bond between 2-PAM and His447 which stabilizes the energy (4*). The intermediate is located in that energy plateau. The DLPNO-CCSD(T) energies show the deprotonation to have a small energetic cost of 2.92 kcal.mol⁻¹ with a small energy barrier of 9.46 kcal.mol⁻¹. In that case the reaction is endothermic as opposed to exothermic but the DLPNO-CCSD(T) does confirm the deprotonation to have a low energetic cost and a small energetic barrier.

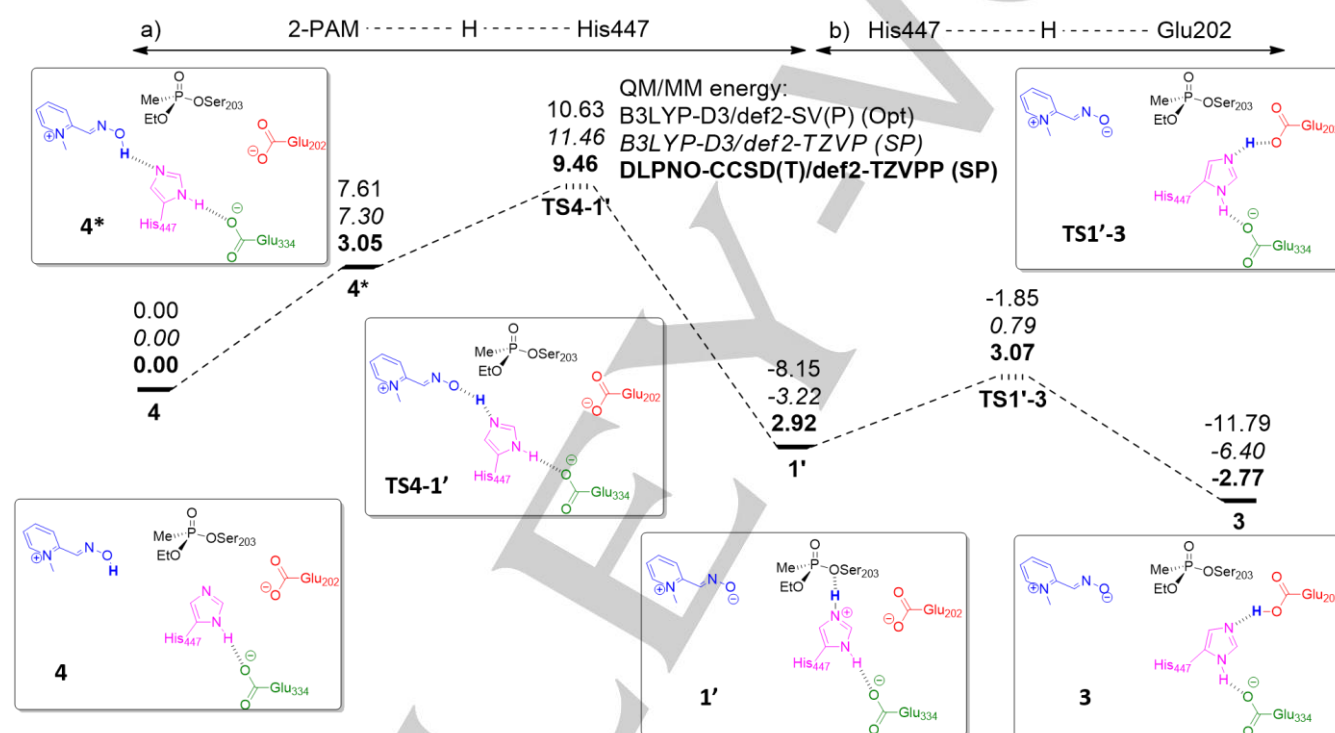


Figure 5. Profile of the deprotonation of 2-PAM by His447 with Glu202 unprotonated. The QM/MM def2-SV(P) optimization energy is in plain text, the QM/MM def2-TZVP single point energy is in italic and the QM/MM DLPNO-CCSD(T)/def2-TZVPP single point energy is in bold. All the energies are in kcal.mol⁻¹.

The deprotonation of 2-PAM by His447 is immediately followed by the deprotonation of His447 by Glu202 Figure 5b. This reaction is also exothermic with a gain of 3.18 kcal.mol⁻¹ between the reactant (1) and the product (3). The energy barrier is only 4.01 kcal.mol⁻¹. There again the DLPNO-CCSD(T) confirms the trends obtained with B3LYP-D3/def2-TZVP. The single points show that the deprotonation of His447 costs 5.69 kcal.mol⁻¹ and has a very small energy barrier of 0.15 kcal.mol⁻¹.

Now that it is known that 2-PAM can be deprotonated by His447 when it is assisted by Glu202 and that this proton can end up on Glu202 in a single exothermic step, we investigated the reaction profile when Glu202 is protonated. In this instance the deprotonation of 2-PAM by His447 is endothermic with the

product's (1P) energy 17.94 kcal.mol⁻¹ higher than the reactant (4P) (Supplemental Figure 4). This deprotonation is a one-step reaction with a 25.44 kcal.mol⁻¹ energy barrier. With DLPNO-CCSD(T) the reaction is also endothermic (27.30 kcal.mol⁻¹) with a very high energy barrier (22.25 kcal.mol⁻¹) (Supplemental Figure 4)

Discussion

First and foremost, the high level ab-initio DLPNO-CCSD(T)/def2-TZVPP results are constantly in line with the

B3LYP-D3/def2-TZVP data. It asserts the pertinence of our DFT approach for the study of this system.

The protonation state of 2-PAM, Glu202 and His447 was shown to have an influence on the reactivation of AChE to be key parameters. As can be seen in the presented results, the protonation state of Glu202 has an effect on both the reactivation and the ability of 2-PAM to lose its proton in the active site of AChE. The protonation state of His447 is also known to be a key element of both the reactivation and the normal enzymatic activity of AChE. Finally, 2-PAM can only reactivate AChE when it is in its oximate form and thus has to

lose a proton at some point of the reactivation process. All possible protonation state combinations for those three elements are enumerated in Figure 6.

Two branches have protonation states that completely exclude the possibility of reactivation. In Branch 1 neither 2-PAM nor His447 nor Glu202 are protonated, which makes reactivation impossible because there is no proton in the system to protonate Ser203 after the elimination of the oxime-VX adduct. In Branch 8, all three are protonated. 2-PAM cannot lose its proton to His447 or Glu202 and be in its active oximate form.

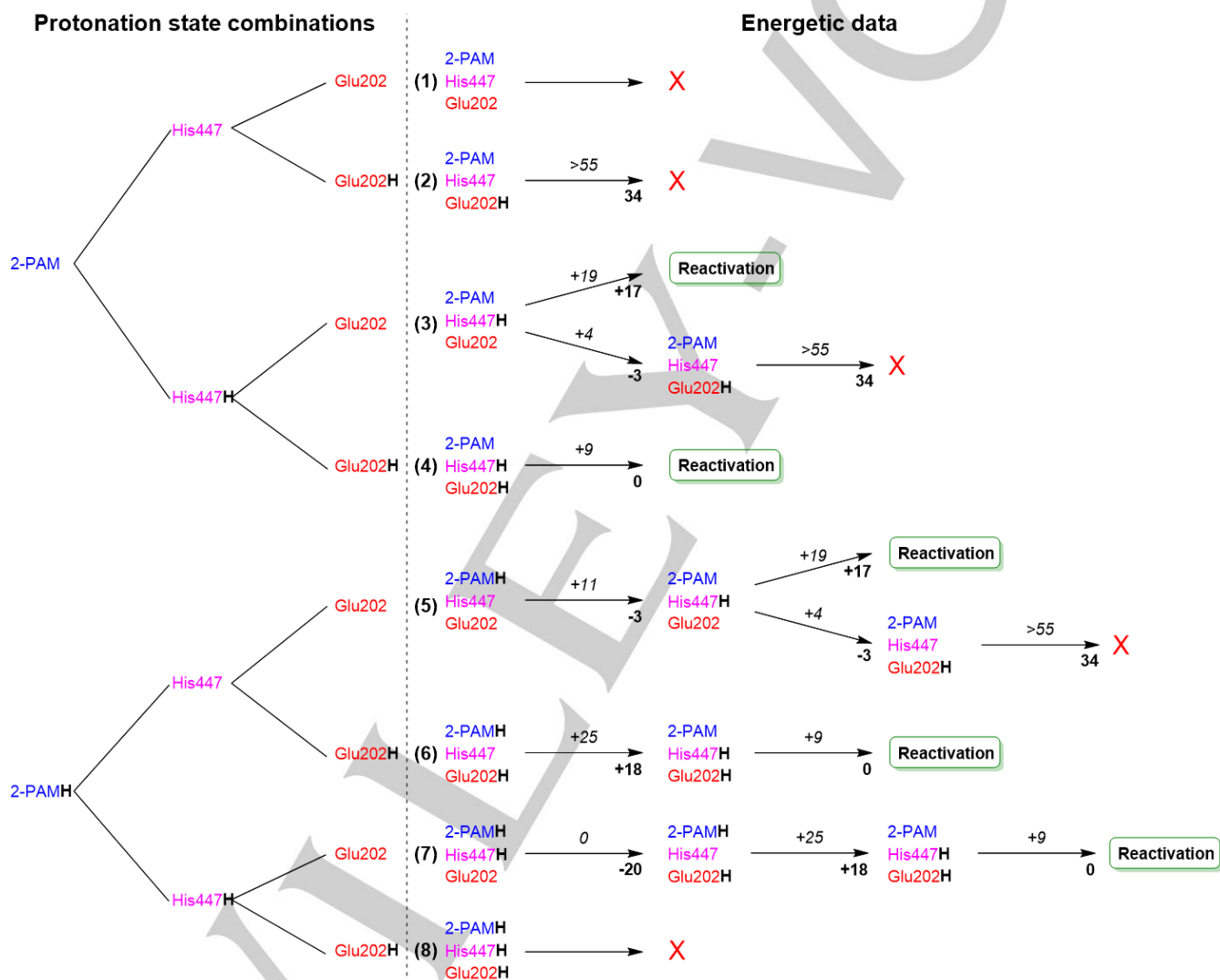


Figure 6. Tree of protonation states of 2-PAM, His447 and Glu202. The reactions are represented by an arrow with the reaction enthalpy at the bottom right and the energy barrier at the top in the middle. The energies are given at the B3LYP-D3/def2-TZVP//CHARMM level in kcal.mol⁻¹ and rounded to the closest integer. At the end of every branch it is indicated whether reactivation occurs or not.

When only Glu202 is protonated (Branch 2) reactivation is impossible. Both the high endothermicity (50.14 kcal.mol⁻¹; at the B3LYP-D3/def2-TZVP//CHARMM level) and the energy barrier,

which is above 55 kcal.mol⁻¹, prevent it. An approximate energy of the product was obtained by putting a constraint on the phosphorus-Ser203 distance but it is not stable. The product

could not be optimized without constraints as the 2-PAM-VX adduct would react instantly on Ser203 to reform the Ser203-VX adduct. Without a proton for Ser203 to capture, the reactivation appears to be impossible.

For Branch 3, when only His447 carries a proton, two reactions are possible. The first is the reactivation of AChE by 2-PAM with the mechanism presented in Figure 3. The second reaction is the proton transfer from His447 to Glu202 (see Figure 5). This second reaction gets us to the starting point of Branch 2 and does not lead to reactivation. The first reaction is endothermic with a $17.00 \text{ kcal.mol}^{-1}$ and a high barrier of $18.90 \text{ kcal.mol}^{-1}$; the second is exothermic with a $3.18 \text{ kcal.mol}^{-1}$ energy gain and an energy barrier of $4.01 \text{ kcal.mol}^{-1}$. The exothermicity and low barrier of the second reaction makes the deprotonation of His447 by Glu202 much more favorable than the reactivation. Branch 3 can thus not lead to reactivation.

When both Glu202 and His447 are protonated (Branch 4) reactivation occurs (see Figure 4). It is isoenergetic ($-0.19 \text{ kcal.mol}^{-1}$) and has a low energy barrier of $8.84 \text{ kcal.mol}^{-1}$.

At the start of Branch 5 only 2-PAM carries a proton. The first reaction that occurs is the proton transfer from 2-PAM to His447. This reaction is slightly exothermic ($3.22 \text{ kcal.mol}^{-1}$) with a low energy barrier of $11.46 \text{ kcal.mol}^{-1}$. After the proton transfer the situation is similar to the start of Branch 3 which, as it was already said, cannot lead to reactivation.

When both 2-PAM and Glu202 are protonated (Branch 6) reactivation can only occur if 2-PAM loses its proton to His447. This deprotonation is endothermic ($17.94 \text{ kcal.mol}^{-1}$) with a barrier of $25.44 \text{ kcal.mol}^{-1}$ (supplemental Figure 4). Once 2-PAM is deprotonated the situation is similar to the start of Branch 4 that does lead to the reaction in one isoenergetic step with a small barrier.

Finally Branch 7 starts with 2-PAM and His447 protonated. Two steps are necessary for reactivation: The deprotonation of His447 by Glu202 and the deprotonation of 2-PAM by His447. The first step is an exothermic reaction ($20.17 \text{ kcal.mol}^{-1}$) with a non-existent energy barrier ($0.01 \text{ kcal.mol}^{-1}$). The second step is the deprotonation of 2-PAM by His447 as described in Branch 6 which lead to reactivation.

Apart from Branch 1 and 8 in Figure 6, which can be directly eliminated, 6 branches remain to discuss. Few other branches can also be disregarded on the basis of the high endergonicity (Branches 2, 3 and 5). Therefore, only 3 protonation states can lead to reactivation (Branches 4, 6 and 7). The common feature of these branches is the fact that two protons are available in the active site. Once these protons end-up on His447 and Glu202, the reactivation barrier is relatively low ($8.84 \text{ kcal.mol}^{-1}$ with the TZVP basis set). With such a low barrier, it appears that AChE reactivation by oximes is merely dependent on the protonation state in the active site rather than closely related to the nucleophilicity of the oximes. Obviously a third parameter is important: binding of the oxime; but this point has been largely addressed by experimental and docking studies.^[22,46,47]

An idealistic case exists for reactivating AChE: oxime enters the gorge deprotonated, and then binds into the active site and His447/Glu202 are both protonated. Since oximes are basic

compounds, this conjunction of protonation states has low probability at normal physiological pH.

In the previous case, the two necessary protons were already present in the active site. Let's now discuss the case when the oxime enters the active site while being protonated, thus bringing one of the two protons. The other proton can thus be located either on His447 or on Glu202. Our calculations indicate that, once the oxime is in the active site, a proton can easily be transferred from His447 to Glu202 (barrier close to zero and high exothermicity). What remains to be done is thus to deprotonate the oxime in order to exacerbate its nucleophilicity and allow for reactivation. This step was found to be energetically costly (barrier of $25.44 \text{ kcal.mol}^{-1}$ and reaction enthalpy of $17.94 \text{ kcal.mol}^{-1}$). Consequently, our computational study indicates that the main problem during the reactivation of inhibited AChE by oximes is not related to the intrinsic nucleophilic strength of the reactivator but rather to its ability to be deprotonated in the active site by the couple His447/Glu202. A strong nucleophilicity is commonly accompanied by a strong basicity. Finding the right oxime is thus balancing between these two contradictory effects for the reactivation process.

The role of Glu202 during the regular catalytic activity of AChE has already been investigated by experimental^[48,49] and theoretical^[13,14,50] means. In particular, it was shown by Monte-Carlo titration on non-inhibited AChE that this glutamic acid is protonated, for all configurations of Ser203. Further EVB calculations also reveal that the kinetics of the deacylation step (Scheme 1, A2) is in line with experiments when this glutamic acid is in its protonated form. On the other hand, many roles were attributed to unprotonated Glu202. For example, it was speculated that charged Glu202 is able to stabilize the binding of ACh by long-range electrostatic interactions.^[51] Also, since His447 is in its protonated state when Ser203 is acetylated, it was conjectured by the same authors that the negative charge of Glu202 would stabilize the positive charge of the doubly protonated imidazole. Some aging mechanisms even considered Glu202 has a possible transient proton acceptor.^[52] Recently, Linusson and Ekström have studied by diffusion trap cryo-rystallography the dynamics of the sarin-inhibited AChE active site in conjunction with HI-6 reactivator.^[53] Notably, they found an interaction between Glu202 and the O-isopropyl moiety of sarin. They also find evidence that a proton transfer occurs close to the rate-limiting step, by deuteration experiments. These findings are in line with our computational analysis. Since it appears that Glu202 is most probably protonated, there is no point to discuss the role of Glu202 as a negatively charged residue but rather to decipher its implication on the structuration and reactivity of the active site, as a neutral side chain. We notice that this residue is highly conserved over the esterase superfamily^[54–56] and we can thus speculate that it is more important than previously thought. Its exact role remains nevertheless elusive.

Conclusion

This computational study reveals for the first time the importance of Glu202 for the reactivation of the normal catalytic activity of AChE. Serine proteases are not characterized by a catalytic triad but by a quartet of residues (Ser203, His337, Glu334 and 202). The roles of both glutamates in the vicinity of Ser203 are of equal importance. Our study also shows that reactivation can occur with oxime entering the active site in its two protonation states. But the occurrence of reactivation depends on the protonation state of the quartet, and particularly on Glu202. Free energy calculations should be performed in order to account for the influence of entropy and also to follow the motions and specific role of water molecules present in the active site. Consequently, our current investigations have shifted to the dynamics of protons exchanges in inhibited AChE by means of constant pH molecular dynamics. In particular, the role of water molecules in the active site as a proton relay between Gu202 and reactivator should be considered.

Acknowledgements

The authors thanks DGA for a Ph.D. grant to T.D.. This work was supported by CNRS, MRES and UPMC.

Keywords: acetylcholinesterase • QM/MM • protonation • reactivation • organophosphate

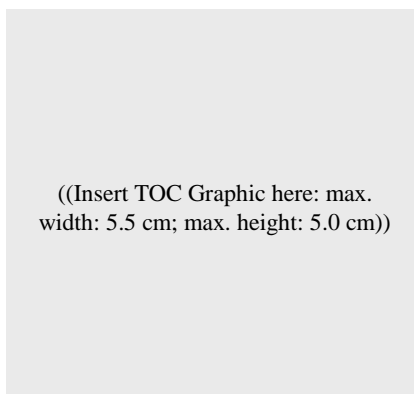
- [1] J. L. Sussman, M. Harel, F. Frolow, C. Oefner, A. Goldman, L. Toker, I. Silman, *Science* **1991**, *253*, 872–879.
- [2] G. Kryger, M. Harel, K. Giles, L. Toker, B. Velan, A. Lazar, C. Kronman, D. Barak, N. Ariel, A. Shafferman, et al., *Acta Crystallogr. D Biol. Crystallogr.* **2000**, *56*, 1385–1394.
- [3] D. M. Quinn, *Chem. Rev.* **1987**, *87*, 955–979.
- [4] J.-P. Colletier, D. Fournier, H. M. Greenblatt, J. Stojan, J. L. Sussman, G. Zaccari, I. Silman, M. Weik, *EMBO J.* **2006**, *25*, 2746–2756.
- [5] T. L. Rosenberry, W. D. Mallender, P. J. Thomas, T. Szegletes, *Chem. Biol. Interact.* **1999**, *119–120*, 85–97.
- [6] Y. Bourne, Z. Radic, G. Sulzenbacher, E. Kim, P. Taylor, P. Marchot, *J. Biol. Chem.* **2006**, *281*, 29256–29267.
- [7] S. Malany, M. Sawai, R. S. Sikorski, J. Seravalli, D. M. Quinn, Z. Radic, P. Taylor, C. Kronman, B. Velan, A. Shafferman, *J. Am. Chem. Soc.* **2000**, *122*, 2981–2987.
- [8] G. Koellner, G. Kryger, C. B. Millard, I. Silman, J. L. Sussman, T. Steiner, *J. Mol. Biol.* **2000**, *296*, 713–735.
- [9] T. C. Marrs, *Pharmacol. Ther.* **1993**, *58*, 51–66.
- [10] M. Trovaslet-Leroy, L. Musilova, F. Renault, X. Brazzolotto, J. Misik, L. Novotny, M.-T. Froment, E. Gillon, M. Loiodice, L. Verdier, et al., *Toxicol. Lett.* **2011**, *206*, 14–23.
- [11] G. Mercey, T. Verdelet, J. Renou, M. Kliachyna, R. Baati, F. Nachon, L. Jean, P.-Y. Renard, *Acc. Chem. Res.* **2012**, *45*, 756–766.
- [12] F. Nachon, E. Carletti, F. Worek, P. Masson, *Chem. Biol. Interact.* **2010**, *187*, 44–48.
- [13] Y. Zhang, J. Kua, J. A. McCammon, *J. Am. Chem. Soc.* **2002**, *124*, 10572–10577.
- [14] Y. Zhou, S. Wang, Y. Zhang, *J. Phys. Chem. B* **2010**, *114*, 8817–8825.
- [15] A. V. Nemukhin, S. V. Lushchekina, A. V. Bochenkova, A. A. Golubeva, S. D. Varfolomeev, *J. Mol. Model.* **2008**, *14*, 409–416.
- [16] J.-L. Fattbert, E. Y. Lau, B. J. Bennion, P. Huang, F. C. Lightstone, *J. Chem. Theory Comput.* **2015**, *11*, 5688–5695.
- [17] J. Wang, J. Gu, J. Leszczynski, *J. Phys. Chem. B* **2006**, *110*, 7567–7573.
- [18] O. Kwasnieski, L. Verdier, M. Malacria, E. Derat, *J. Phys. Chem. B* **2009**, *113*, 10001–10007.
- [19] H. M. Senn, W. Thiel, *Angew. Chem. Int. Ed.* **2009**, *48*, 1198–1229.
- [20] M. G. Quesne, T. Borowski, S. P. de Visser, *Chem. - Eur. J.* **2016**, *22*, 2562–2581.
- [21] Y. Li, L. Du, Y. Hu, X. Sun, J. Hu, *Can. J. Chem.* **2012**, *90*, 376–383.
- [22] R. Lo, N. B. Chandar, M. K. Kesharwani, A. Jain, B. Ganguly, *PLoS ONE* **2013**, *8*, e79591.
- [23] R. Lo, B. Ganguly, *Mol. Biosyst.* **2014**, *10*, 2368–2383.
- [24] K. S. Matos, D. T. Mancini, E. F. da Cunha, K. Kuča, T. C. França, T. C. Ramalho, *J. Braz. Chem. Soc.* **2011**, *22*, 1999–2004.
- [25] J. O. S. Giacoppo, T. C. C. França, K. Kuča, E. F. F. da Cunha, R. Abagyan, D. T. Mancini, T. C. Ramalho, *J. Biomol. Struct. Dyn.* **2015**, *33*, 2048–2058.
- [26] J. Liu, Y. Zhang, C.-G. Zhan, *J. Phys. Chem. B* **2009**, *113*, 16226–16236.
- [27] Y. Ashani, Z. Radic, I. Tsigelny, D. C. Vellom, N. A. Pickering, D. M. Quinn, B. P. Doctor, P. Taylor, *J. Biol. Chem.* **1995**, *270*, 6370–6380.
- [28] E. Carletti, H. Li, B. Li, F. Ekström, Y. Nicolet, M. Loiodice, E. Gillon, M. T. Froment, O. Lockridge, L. M. Schopfer, et al., *J. Am. Chem. Soc.* **2008**, *130*, 16011–16020.
- [29] B. R. Brooks, C. L. Brooks, A. D. Mackerell, L. Nilsson, R. J. Petrella, B. Roux, Y. Won, G. Archontis, C. Bartels, S. Boresch, et al., *J. Comput. Chem.* **2009**, *30*, 1545–1614.
- [30] A. D. Mackerell, M. Feig, C. L. Brooks, *J. Comput. Chem.* **2004**, *25*, 1400–1415.
- [31] MacKerell A. D., D. Bashford, M. Bellott, Dunbrack R. L., J. D. Evanseck, M. J. Field, S. Fischer, J. Gao, H. Guo, S. Ha, et al., *J. Phys. Chem. B* **1998**, *102*, 3586–3616.
- [32] E. F. Pettersen, T. D. Goddard, C. C. Huang, G. S. Couch, D. M. Greenblatt, E. C. Meng, T. E. Ferrin, *J. Comput. Chem.* **2004**, *25*, 1605–1612.
- [33] M. H. M. Olsson, C. R. Søndergaard, M. Rostkowski, J. H. Jensen, *J. Chem. Theory Comput.* **2011**, *7*, 525–537.
- [34] P. Sherwood, A. H. de Vries, M. F. Guest, G. Schreckenbach, C. R. A. Catlow, S. A. French, A. A. Sokol, S. T. Bromley, W. Thiel, A. J. Turner, et al., *J. Mol. Struct. THEOCHEM* **2003**, *632*, 1–28.
- [35] R. Ahlrichs, M. Bär, M. Häser, H. Horn, C. Kölmel, *Chem. Phys. Lett.* **1989**, *162*, 165–169.
- [36] R. Ahlrichs, F. Furche, C. Hättig, W. Klopper, M. Sierka, F. Weigend, *TURBOMOLE*, TURBOMOLE GmbH, Development of University of Karlsruhe and Forschungszentrum Karlsruhe GmbH, **2012**.
- [37] A. D. Becke, *J. Chem. Phys.* **1993**, *98*, 5648–5652.
- [38] C. Lee, W. Yang, R. G. Parr, *Phys. Rev. B* **1988**, *37*, 785–789.
- [39] S. Grimme, J. Antony, S. Ehrlich, H. Krieg, *J. Chem. Phys.* **2010**, *132*, 154104.
- [40] F. Weigend, R. Ahlrichs, *Phys. Chem. Chem. Phys.* **2005**, *7*, 3297.
- [41] F. Neese, *Wiley Interdiscip. Rev. Comput. Mol. Sci.* **2012**, *2*, 73–78.
- [42] C. Riplinger, F. Neese, *J. Chem. Phys.* **2013**, *138*, 34106.
- [43] C. Riplinger, B. Sandhoefer, A. Hansen, F. Neese, *J. Chem. Phys.* **2013**, *139*, 134101.
- [44] D. G. Liakos, M. Sparta, M. K. Kesharwani, J. M. L. Martin, F. Neese, *J. Chem. Theory Comput.* **2015**, *11*, 1525–1539.
- [45] O. V. Gritsenko, B. Ensing, P. R. T. Schipper, E. J. Baerends, *J. Phys. Chem. A* **2000**, *104*, 8558–8565.
- [46] M. Kliachyna, G. Santoni, V. Nussbaum, J. Renou, B. Sanson, J.-P. Colletier, M. Arboléas, M. Loiodice, M. Weik, L. Jean, et al., *Eur. J. Med. Chem.* **2014**, *78*, 455–467.
- [47] J. Renou, J. Dias, G. Mercey, T. Verdelet, C. Rousseau, A.-J. Gastellier, M. Arboléas, M. Touvrety-Loiodice, R. Baati, L. Jean, et al., *RSC Adv.* **2016**, *6*, 17929–17940.
- [48] G. Gibney, S. Camp, M. Dionne, K. MacPhee-Quigley, P. Taylor, *Proc. Natl. Acad. Sci.* **1990**, *87*, 7546–7550.
- [49] Z. Radic, G. Gibney, S. Kawamoto, K. MacPhee-Quigley, C. Bongiorno, P. Taylor, *Biochemistry (Mosc.)* **1992**, *31*, 9760–9767.
- [50] P. Vagedes, B. Rabenstein, J. Åqvist, J. Marelis, E.-W. Knapp, *J. Am. Chem. Soc.* **2000**, *122*, 12254–12262.
- [51] S. T. Wlodek, J. Antosiewicz, J. M. Briggs, *J. Am. Chem. Soc.* **1997**, *119*, 8159–8165.
- [52] C. Viragh, R. Akhmetshin, I. M. Kovach, C. Broomfield, *Biochemistry (Mosc.)* **1997**, *36*, 8243–8252.
- [53] A. Allgardsson, L. Berg, C. Akfur, A. Hörnberg, F. Worek, A. Linusson, F. J. Ekström, *Proc. Natl. Acad. Sci.* **2016**, *113*, 5514–5519.
- [54] J. C.-H. Chen, L. J. W. Miercke, J. Krucinski, J. R. Starr, G. Saenz, X. Wang, C. A. Spilburg, L. G. Lange, J. L. Ellsworth, R. M. Stroud, *Biochemistry (Mosc.)* **1998**, *37*, 5107–5117.
- [55] V. A. de Souza, D. J. Scott, J. E. Nettleship, N. Rahman, M. H. Charlton, M. A. Walsh, R. J. Owens, *PLoS ONE* **2015**, *10*, e0143919.
- [56] B. Spiller, A. Gershenson, F. H. Arnold, R. C. Stevens, *Proc. Natl. Acad. Sci. U. S. A.* **1999**, *96*, 12305–12310.

Entry for the Table of Contents (Please choose one layout)

Layout 1:

FULL PAPER

Text for Table of Contents



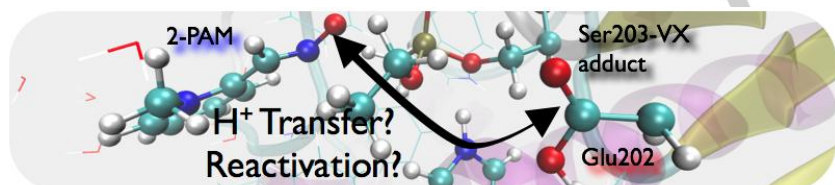
Author(s), Corresponding Author(s)*

Page No. – Page No.

Title

Layout 2:

FULL PAPER



Proton transfer during reactivation of organophosphate inhibited acetylcholinesterase were investigated by QM/MM calculations. They reveal an interplay between the protonation states of the catalytic triad and a glutamate closed to the active site, which needs first to be protonated for reactivation to occur.

Thomas Driant, Florian Nachon, Cyril Ollivier, Pierre-Yves Renard, Etienne Derat*

Page No. – Page No.

On the influence of the protonation states of active site residues on AChE reactivation: a QM/MM approach